



**Tunable Optical Metamaterial-Based Sensors Enabled by
Closed Bipolar Electrochemistry**

| | |
|-------------------------------|--|
| Journal: | <i>Analyst</i> |
| Manuscript ID | AN-ART-06-2019-001137.R1 |
| Article Type: | Paper |
| Date Submitted by the Author: | 19-Aug-2019 |
| Complete List of Authors: | Crouch, Garrison; University of Notre Dame, Oh, Christiana; University of Notre Dame Fu, Kaiyu; Stanford University, Department of Radiology Bohn, Paul; University of Notre Dame, Department of Chemical and Biomolecular Engineering |
| | |

1
2
3
4
5
6 **Tunable Optical Metamaterial-Based Sensors Enabled by Closed Bipolar Electrochemistry**
7
8
9

10
11
12 Garrison M. Crouch,¹ Christiana Oh,¹ Kaiyu Fu,² Paul W. Bohn^{1,2*}
13
14

15
16
17
18 ¹Department of Chemical and Biomolecular Engineering, University of Notre Dame, Notre
19
20 Dame, IN 46556
21

22 ²Department of Chemistry and Biochemistry, University of Notre Dame, Notre Dame, IN 46556
23
24
25
26
27
28
29
30
31
32
33
34
35
36
37
38
39
40
41
42
43
44
45
46

47 *Author to whom correspondence should be addressed,
48

49 *pbohn@nd.edu*, Tel.: +1 574 631 1849; Fax: +1 574 631 8366
50
51
52
53
54
55
56
57
58

ABSTRACT

Enabled by the proliferation of nanoscale fabrication techniques required to create spatially-repeating, sub-wavelength structures to manipulate the behavior of visible-wavelength radiation, optical metamaterials are of increasing interest. Here we develop and characterize a chemical sensing approach based on electrochemical tuning of the optical response function of large-area, inexpensive nanoaperture metamaterials at visible and near-IR wavelengths. Nanosphere lithography is used to create an ordered array of sub-wavelength apertures in a Au film. The spacing of these apertures is established during fabrication, based on the size of the polystyrene nanospheres. Tunable shifts in the transmission spectrum can be produced post-fabrication by electrodeposition of a dissimilar metal, Ag, using the nanoaperture film as one electrode in a 2-electrode closed bipolar electrochemical (CBE) cell, altering hole size, film thickness, and film composition while maintaining hole spacing dictated by the original pattern. Optical transmission spectra acquired under galvanostatic conditions can be expressed as a linear combination of the initial and final (saturated) spectra, and the resulting response function exhibits a sigmoidal response with respect to the amount of charge (or metal) deposited. This architecture is then used to perform optical coulometry of model analytes in a CBE-based analyte-reporter dual cell device, thus expanding the capability of CBE-based sensors. Increasing the exposed electrode area of the analyte cell increases the response of the device, while modifying the circuit resistance alters the balance between sensitivity and dynamic range. These tunable nanoaperture metamaterials exhibit enhanced sensitivity compared to CBE electrochromic reporter cells to the μM to nM concentration range, suggesting further avenues for development of CBE-based chemical sensors as well as application to inexpensive, point-of-care diagnostic devices.

Introduction

Improved sensitivities and fast response times have followed developments in functional biomaterials, and advances in fabrication have yielded biosensors in which biomolecular and electronic components are integrated.¹⁻⁴ Electrochemical biosensors, in particular, frequently combine a bio-recognition element with electrochemical transduction.^{5, 6} In this regard, there is great interest in pursuing novel methods of reading out the bio-recognition event, and nature suggests a novel route to do so. For example, the brilliantly iridescent wing of the Morphinae butterfly is a well-known natural example of an optical metamaterial – a nanostructured material that exploits repetitive interactions of light to create structural color from a colorless bulk material - in the case of the butterfly, a striking blue that does not fade with time or exposure to light.⁷

Materials which utilize subwavelength structures to direct the propagation of electromagnetic radiation, in ways not available to bulk materials, are the subject of intense current research⁸ due to exciting capabilities presented by non-classical optical phenomena, *e.g.* negative refractive index materials for cloaking.⁹ A particularly accessible category of subwavelength metamaterial structures is based on spatially repeating nanoapertures, which can access a wide range of optical properties depending on the hole size, spacing, geometry, and metallic film thickness.¹⁰ For example, single, or distantly-spaced, nanoapertures, may exhibit zero-mode waveguide behavior and block propagating modes of light, a property which has been used for single-molecule fluorescence studies.¹¹ In larger, more closely-spaced arrays, nanoaperture-based metamaterials may exhibit extraordinary optical transmission,¹² useful in applications including bandpass optical filters¹³ and direct chemical sensing.¹⁴ A particularly appealing top-down, massively-parallel fabrication strategy to achieve these closely-spaced arrays is based on nanosphere

1
2
3 lithography (NSL) - first developed for producing nanopillar arrays¹⁵ and then later extended to
4
5 nanoaperture arrays by adding an etch step.^{16, 17}
6
7

8 The work described here exploits the characteristic optical response function of
9
10 nanoaperture-based metamaterials to achieve electrochemically-tunable electrochromic behavior
11
12 for chemical sensing. The spectral changes of nanoaperture metamaterials is not due to a change
13
14 in the underlying electronic structure. Instead, the morphology of the architecture is altered
15
16 through the electrodeposition of a dissimilar metal, thus altering the size of the holes in the array
17
18 and the nature of the composite metallic architecture. This is philosophically similar, yet nearly
19
20 opposite in implementation, to the approach recently demonstrated by Wang and Chu, *et. al.*,¹⁸ in
21
22 which a tunable metamaterial was realized *via* electrodeposition of silver onto gold nanodots.
23
24
25
26

27 In this work, we utilize closed bipolar electrochemistry (CBE) - an effective method to
28
29 exploit the unique properties of non-powered, electrified interfaces.¹⁹⁻²² Prior work from our
30
31 laboratory^{23, 24} established a two-cell CBE device, in which the analyte-targeted redox reaction
32
33 (analyte cell) was physically separated from the readout mechanism (reporter cell). In the first
34
35 version of the device, the reporter cell employed a readout based on the electrochromic reduction
36
37 of colorless methyl viologen dication, MV^{2+} , to its purple, radical cation, $MV^{+\bullet}$. In the present
38
39 work, we develop a new concept for sensor readout by replacing the electrochromic reaction
40
41 with a NSL-fabricated nanoaperture metal metamaterial, the transmission spectrum of which is
42
43 then altered by electrodeposition or electrodisolution of Ag, thereby effecting structure-based
44
45 color changes. Since the change in the transmission spectrum is a function of the amount of Ag
46
47 deposited, the nanoaperture array can be used to correlate the magnitude of the optical readout to
48
49 the amount of charge transferred, thus translating coulometric efficiency of the analytical
50
51 reaction to a measurable shift in the optical transmission spectrum. Both the transmission
52
53
54
55
56
57
58
59
60

1
2
3 spectrum as well as the maximum transmitted intensity change may be described by a sigmoidal
4 sensor-response curve. Proof-of-principle for this sensing scheme is demonstrated by using
5 nanoapertured Au to detect $\text{Fe}(\text{CN})_6^{4-}$ down to 10 μM in standard cells, extending to 10 nM with
6 special cell design and series resistance to control the rate of charge transfer.
7
8
9
10
11

12 13 **Experimental Section**

14
15
16 *Metamaterial Fabrication and Characterization.* NSL was used to create nanoapertured
17 metamaterials with different hole sizes and spacings to tune the optical response. Polystyrene
18 beads in aqueous solution with mean diameter of 0.6 μm were obtained from Sigma-Aldrich and
19 used as received. Beads were mixed 1:1 in ethanol, then pipetted into a glass dish filled with DI
20 water ($\rho \sim 18.2 \text{ M}\Omega \text{ cm}$, Millipore) to form a self-assembled monolayer.²³ Glass slides (Schott)
21 were treated in O_2 plasma prior to immersion in the solution. After transfer of the monolayer
22 onto the glass, beads were etched via O_2 plasma (Plasma Therm 790 RIE) and 50 nm Au with 5
23 nm Ti was deposited by e-beam evaporation (Oerlikon.) Transmission measurements were
24 performed, as shown in **Figure S1** (Supplemental Information, SI), using a fiber-coupled,
25 stabilized tungsten lamp (ThorLabs, SLS202L) which was expanded and passed through neutral
26 density filters before being focused on the sample. The sample was placed at the focal plane of
27 the illumination path, with transmitted light collected and coupled into a multi-mode optical fiber
28 from which it was directed into a grating spectrometer (Princeton Instruments, Acton SpectraPro
29 SP-2750) fitted with a PyLoN cryogenically-cooled CCD camera. Spectra were acquired in
30 LightField and imported into Matlab (2018b) for further processing.
31
32
33
34
35
36
37
38
39
40
41
42
43
44
45
46
47
48
49

50
51 *Electrodeposition.* Polyvinyl butyral (PVB), copper (II) chloride, tetrabutylammonium
52 bromide (TBABr), silver nitrate (AgNO_3), and dimethyl sulfoxide (DMSO) were ordered from
53
54
55
56
57
58

1
2
3 Sigma-Aldrich and used as received. The electrodeposition solution was designed after a
4
5 composition previously reported to produce optically-reflective Ag films,²⁵ but with CuCl₂,
6
7 AgNO₃, and TBABr concentrations increased to decrease the overpotential required to yield
8
9 practical deposition rates. Solutions used in these experiments were 12 mM AgNO₃, 2.4 mM
10
11 CuCl₂, and 50 mM TBABr with 10 wt% PVB in DMSO. Electrodeposition was controlled with a
12
13 Gamry Reference 600 potentiostat in a 2-electrode configuration with an ITO-coated glass slide
14
15 as the quasi-reference/counter electrode (QRCE).
16
17
18

19
20 *Analyte and Reporter Cell and CBE Configuration.* Sensor devices were constructed with
21
22 separate analyte and reporter cells connected by a CBE, as shown schematically in **Figure S1(a)**.
23
24 The analyte cell was constructed using a standard glass slide (VWR) coated with Ti/Pt (10
25
26 nm/100 nm), a tape spacer (50 μm, Scotch), and an ITO-coated glass slide (Sigma, 8-12 Ω/sq). A
27
28 4 mm hole punched in the tape spacer created the containment volume for the analyte solution,
29
30 which was overfilled (10 μL) prior to assembly. Potassium ferrocyanide (Fe(CN)₆⁴⁻) (Fisher
31
32 Scientific) was used as received and dissolved in deionized water (18.2 MΩ cm, Millipore) with
33
34 0.1 M KCl supporting electrolyte (Sigma Aldrich). The reporter cell consisted of the
35
36 nanoaperture metamaterial, as described above, along with two glass microscope slide spacers
37
38 (Schott), and an ITO-coated glass slide, with Teflon tape (Uline) to prevent leakage. Holes of
39
40 diameters *ca.* 4 mm and 6 mm, were drilled in spacers 1 and 2, respectively, with a channel
41
42 milled in spacer 2 to allow injection of the electrodeposition solution *via* syringe after device
43
44 assembly. Cells were clamped with sufficient pressure to prevent leakage. *In situ* optical
45
46 measurements of the reporter cell were performed in a custom measurement apparatus, shown in
47
48 **Figure S1(b)**, using transmission reference spectra acquired with a bare glass slide, instead of
49
50 the nanoaperture metamaterial. The Pt-coated glass slide of the analyte cell was used as the
51
52
53
54
55
56
57
58
59
60

1
2
3 working electrode, with the ITO slide of the reporter cell as the QRCE. An insulated Al-core
4 wire was affixed to the nanoaperture material of the reporter cell and the ITO slide of the
5 analytical cell to create the CBE.
6
7
8
9

10 **Results and Discussion**

11
12
13 *Optical Response of Nanoapertured Metamaterials.* NSL is a facile method for producing
14 large-area, well-ordered nanoaperture arrays for electrochemical and optical applications.²⁶
15 Aperture spacing and size may be manipulated by changing the size of nanospheres used to
16 template the array and the O₂ plasma etch time, respectively. Prior to O₂ plasma etching, removal
17 of the polystyrene spheres yielded a film consisting of discontinuous trigonal nanopylramids.²⁷
18 To examine the change in optical transmission as a function of nanoaperture size while
19 maintaining aperture spacing, the O₂ plasma etch time was varied in more granular steps, with
20 transmission spectra taken after the initial onset of film conductivity (30 s etch time) as shown in
21 **Figure 1**. First, an overall decrease in transmission is observed with decreasing aperture size,
22 which is reasonable given the increasing proportion of metal to clear aperture area. Aperture
23 areas measured by plan view SEM and analyzed with ImageJ are plotted in **Figure S2** and show
24 that the radii of nanoapertures arrays can be tuned from 287 nm to 227 nm for etch times from 40
25 s to 2 min, respectively. These limits were selected consistent with the onset of film conductivity
26 at ~30 s etch time. At etch times exceeding 2 min, the beads used for NSL templating were
27 damaged and difficult to remove. The peak in transmission near 500 nm, **Figure 1(a)**, is
28 attributed to bulk Au,²⁸ while the gradual transition from a relatively flat response at wavelengths
29 >600 nm to a distinct peak centered at ~1000 nm is attributed to the evolution of nanoaperture
30 structure, as are less pronounced peaks at *ca.* 700 nm and 1625 nm. Because all of these
31 transmission peaks are at wavelengths greater than twice the diameter of the apertures in the
32
33
34
35
36
37
38
39
40
41
42
43
44
45
46
47
48
49
50
51
52
53
54
55
56
57
58
59
60

1
2
3 metamaterial, shifts in these peaks are attributed to differences in nanoaperture structure.²⁸
4
5

6 *Post-Fabrication Tunability.* The ability to tune the nanoaperture metamaterial structure
7
8 post-fabrication is critical to the proposed mechanism for optical coulometry in the assembled
9
10 CBE device. The effect of metal electrodeposition onto an idealized nanoaperture array was
11
12 simulated using a 3-dimensional finite-element simulation (COMSOL) - required due to the
13
14 hexagonal lattice structure. In this simulation, a complete unit cell was modeled using a 50 nm
15
16 Au film at the glass-air interface with 580 nm diameter apertures on a 600 nm pitch hexagonal
17
18 lattice and with Floquet periodicity at the boundaries. Transmission was computed for each
19
20 frequency and, as shown in **Figure S3**, the calculated transmission spectrum transitions from
21
22 relatively flat in the infrared with 5 nm of Ag to exhibit a well-defined peak at ~850 nm with
23
24 increasing Ag thickness, the emergent near-IR peak at ~850 nm being a key feature which was
25
26 selected for experimental study.
27
28
29
30
31

32 To experimentally characterize the kinetics of the optical changes, a reporter cell was
33
34 assembled with the nanoaperture metamaterial connected to the potentiostat as the working
35
36 electrode, with the ITO slide acting as a QRCE. An initial blank transmission spectrum was
37
38 acquired with a glass slide of the same type as the nanoaperture metamaterial substrate. In
39
40 addition, an initial spectrum with an as-fabricated nanoaperture metamaterial was acquired to
41
42 establish a $t = 0$, $Q = 0$ baseline before any charge, Q , was passed. Galvanostatic conditions were
43
44 then established with 20 μ A current applied for specified increments up to a maximum of 300 s.
45
46 After each application, a transmission spectrum was acquired, as shown in **Figure 2(a)**. **Figures**
47
48 **2(b)** and **2(c)** demonstrate the reduction in nanoaperture radius before and after Ag deposition.
49
50 Comparing these spectra to the simulation results in **Figure S3**, the experimental spectra show
51
52 the same general spectral bands and trends with thickness, although broader and red-shifted. The
53
54
55
56
57
58

1
2
3 broadening of the experimental peaks is likely due to fabrication nonidealities, as literature
4 suggests that parameters such as metal film roughness,²⁹ scattering from metal and dielectric
5 imperfections,³⁰ , and slight hole size differences³¹ are causes of resonance peak broadening.
6
7 Also of note are the gradual disappearance of the peak at 500 nm (attributed to bulk Au),
8 indicating that electrodeposited Ag gradually covers the Au NSL-derived template with
9
10 thicknesses approaching the 40-60 nm, as well as a redshift of the near-IR peak at *ca.* 900 nm.
11
12 The total experimental red-shift is estimated to be $\Delta\lambda \sim 41$ nm, while the simulations give
13
14 $\Delta\lambda \sim 36$ nm (from 60 nm to 100 nm Ag). This observation is consistent with the growth of the
15
16 Ag intensity in the energy-dispersive x-ray (EDX) images given in **Figures S3** and **S4**, acquired
17
18 before and after Ag deposition. The main result of both simulations and experiments is that the
19
20 near-IR feature identified in **Figures 2** and **S2** becomes more pronounced with increasing Ag
21
22 deposition.
23
24
25
26
27
28
29
30
31

32 To obtain a metric for sensor response, the transmission spectra were first normalized to unit
33 area to account for the decrease in transmission with increasing Ag deposition, the result being
34 termed the intensity response. Each normalized spectrum was then fit to a linear combination of
35 the starting ($t = 0$ s, S_0) and ending ($t = 300$ s, S_{300}) spectra, with a single variable, x , governing
36 the relative weighting, *i.e.*
37
38
39
40
41
42
43

$$S(t) = xS_{300} + (1 - x)S_0 \quad (1)$$

44
45
46 Plotting this variable against the cumulative deposition time in a galvanostatic experiment, as
47 shown in **Figure 3**, yields a sigmoidal sensor-response curve.³² The charge transferred from
48 analytical to reporter cell, Q , can be calculated from the galvanostatic current, i , and the
49 deposition time t_{dep} as:
50
51
52
53
54
55
56
57
58
59
60

$$Q = \int_0^t i dt = 20 \mu A * t_{dep} \quad (2)$$

Because the current is constant in a galvanostatic experiment, we conclude that the sensor exhibits a large response range from 0 to 6 mC (*i.e.* $t = 0$ to 300 s). Similarly, the overall change in intensity of each spectrum can be plotted *vs.* deposition time, which produces a similar sigmoidal response curve. A sigmoidal curve was fit to the average of the two response metrics to define an overall sensor response, SR:

$$SR = \left(\frac{A}{1 + e^{-B*(Q-C)}} + D \right) \quad (3)$$

where Q is the charge transferred, A is a scaling factor, D is a constant, and B and C are the spread and offset of the sigmoid function, respectively.

CBE Device Response with Model Analyte. To assess the capability of the nanoaperture metamaterial-based reporter to function in variable concentration chemical sensing measurements, the CBE device was assembled as shown in **Figure S1**, and a constant potential (in contrast to the constant current experiments described above) was applied using the Pt electrode of the analyte cell as the working electrode. In this implementation, the ITO-wire-nanoaperture metamaterial (reporter side) functioned as the CBE. To find the correct time and voltage conditions for optimum sensing, 1 mM $\text{Fe}(\text{CN})_6^{4-}$ was introduced to the analyte cell, and optical spectra were recorded at increasing time intervals. After a cumulative 10 min application of -2.0 V (Pt WE *vs.* ITO QRCE), the sensor was nearly saturated, although some response was still obtained upon a further 5 min application - 900 s total, **Figure 4(a)**. The normalized spectra were again expressed as a linear combination of the initial (0 s) and saturated (900 s) spectra, and the spectral progression is shown as a function of cumulative charge in **Figure 4(b)**.

1
2
3 *CBE Sensor Range.* Using the voltage application time required to reach near-saturation of
4 the reporter cell at 1 mM Fe[(CN)₆]⁴⁻, further tests were conducted to examine the performance
5 of the NSL-based reporter cell using lower concentrations of Fe[(CN)₆]⁴⁻ in the analyte cell. For
6 these experiments, the concentration was stepped from 1 μM to 1 mM in quarter- and half-
7 decade increments, with -2.0 V applied across the assembled CBE device for 7 min. The sensor
8 response was observed to be below the noise floor from 1 μM to 25 μM, before increasing
9 substantially, *viz.* **Figure 5.**

10
11
12
13
14
15
16
17
18
19
20 The limiting current for a parallel planar electrode configuration, such as the one used here,
21 is:

$$i_{\text{lim}} = \frac{nFADC}{z} \quad (3)$$

22
23
24
25
26
27
28
29
30 where n = number of electrons transferred, F = Faraday constant, A = overlapping electrode area,
31 D = diffusion coefficient, C = concentration of electroactive species, and z = electrode
32 separation. The linearity is an obvious advantage in many kinds of experiments, but in the optical
33 coulometry approach taken here it presents a challenge. For example, if a linear dynamic range
34 from 1 μM to 1 mM is desired, the error in the optical readout of the nanoaperture material must
35 be <<0.1%, which is smaller than the noise floor observed upon optical readout of the reporter
36 cell. If the sensing paradigm is changed such that the time is measured to achieve a desired
37 sensor response and 1 mM is measured at 30 s, then detection of 1 μM would require more than
38 8 h. Obviously either scenario presents problems.

39
40
41
42
43
44
45
46
47
48
49
50
51 To address this conundrum, we implemented two changes. First, the noise floor which limits
52 the measurements shown in **Figure 5** was addressed through a combination of lowering the
53

1
2
3 applied potential and increasing the analyte cell area. In addition, we added a series resistance to
4
5 the CBE thus limiting the current at higher concentrations, designing the experiment for a
6
7 constant analysis time of 1 h, rather than constant current or voltage. As shown in **Table 1**, a
8
9 monotonic response was obtained over the analyte concentration range 100 nM - 10 μ M, thus
10
11 extending the viable concentration range of the CBE-enabled optical metamaterial approach.
12
13 While 1 h experiment times are prohibitive, these results point the way to the proper combination
14
15 of cell geometry and electrochemical driving forces to permit high sensitivity chemical sensing
16
17 using the CBE-enabled metamaterials approach.
18
19
20
21

22
23 Once an experiment (or multiple experiments) is completed, the nanoaperture metamaterial
24
25 may be removed from the reporter cell. Excess electrolyte may be removed via a rinse with
26
27 acetone and dried under a stream of N₂, while preserving the electrodeposited silver film and the
28
29 resulting Ag-decorated nanoaperture metamaterial. This provides a physical artifact that can act
30
31 as a record of the test that was performed, which is a distinct advantage over redox-based
32
33 electrochromic readouts^{23, 24} in which the reporter compound (methyl viologen) returns to a
34
35 colorless state after the applied voltage bias is removed. The results of the test are easily
36
37 observed visually and by imaging. Alternatively, the silver film may be removed by immersion
38
39 in a wet etchant (*e.g.* Cr Etch, Sigma Aldrich) without damaging the underlying Au film, thus
40
41 allowing the substrate to be re-used.
42
43
44
45

46 **Conclusions**

47
48
49 Post-fabrication tuning of the optical response function of metamaterials is a potentially
50
51 powerful method to increase their application to a wide range of problems, specifically as
52
53 demonstrated here, in chemical sensing. In this work, a large-area, tunable optical nanoaperture-
54
55 based metamaterial was fabricated using scalable, inexpensive NSL. By manipulating both
56
57
58
59

1
2
3 aperture size and spacing through easily-accessible process parameters, we demonstrated post-
4
5 fabrication tuning of metamaterial optical response function and correlated the mechanism of
6
7 tuning - charge transfer via electrodeposition - to a repeatable chemical sensor response. This
8
9 response was leveraged by coupling the nanoaperture metamaterial to an analytical redox
10
11 reaction using closed bipolar electrochemistry. The results suggest possible application of this
12
13 metamaterial-based readout to point-of-care diagnostics devices, as the device configuration
14
15 exhibits several distinct advantages for electrochemical biosensing and field-deployable testing.
16
17 The CBE geometry physically separates the two electrochemical cells, thus minimizing cross-
18
19 talk between the sensing and reporting systems and allows for remote control or detection.
20
21 Further, the device can be extended to multiplex operation by combining multiple sets of
22
23 analyte/reporter cell systems in parallel for simultaneous determination of several analytes.
24
25 Finally, the device provides a means for electrochemical detection using a metamaterial-based
26
27 optical reporter, thereby filling the sensitivity gap between fluorescent and colorimetric
28
29 reporters.
30
31
32
33
34
35

36 **Acknowledgements**

37
38
39 This work was supported through a NASA Space Technology Research Fellowship (GMC,
40
41 NNX16AM45H), and the Department of Energy (CO, DE FG02 07ER1585.) We thank Prof.
42
43 Anthony Hoffman for the use of his optics lab and equipment. The authors also thank Irfan Khan
44
45 for helpful discussions and preliminary data collection, and Galen Harden for instruction and
46
47 troubleshooting of the spectrometer, and Seung-Ryong Kwon for assistance with sample
48
49 fabrication and discussions concerning simulation results. Fabrication and structural
50
51 characterization of the devices were performed the Notre Dame Nanofabrication Facility and the
52
53
54
55
56
57
58

1
2
3 Notre Dame Integrated Imaging Facility, respectively, whose generous support is gratefully
4
5 acknowledged.
6
7

8 **References**

- 9
10
11 1. D. W. Kimmel, G. LeBlanc, M. E. Meschievitz and D. E. Cliffel, *Analyt. Chem.*, 2012,
12 **84**, 685-707.
13
14
15
16
17 2. A. P. F. Turner, *Chem. Soc. Rev.*, 2013, **42**, 3184-3196.
18
19
20 3. D. Sarkar, W. Liu, X. J. Xie, A. C. Anselmo, S. Mitragotri and K. Banerjee, *ACS Nano*,
21 2014, **8**, 3992-4003.
22
23
24
25
26 4. M. Li, L. Shi, T. Xie, C. Jing, G. Xiu and Y.-T. Long, *ACS Sensors*, 2017, **2**, 263-267.
27
28
29 5. N. J. Ronkainen, H. B. Halsall and W. R. Heineman, *Chem. Soc. Rev.*, 2010, **39**, 1747-
30 1763.
31
32
33
34
35 6. Y. Y. Shao, J. Wang, H. Wu, J. Liu, I. A. Aksay and Y. H. Lin, *Electroanalysis*, 2010,
36 **22**, 1027-1036.
37
38
39
40 7. S. Kinoshita, S. Yoshioka, Y. Fujii and N. Okamoto, *Forma*, 2002, **17**, 103-121.
41
42
43
44 8. M. Francesco and A. Andrea, *Chin. Phys. B*, 2014, **23**, 047809.
45
46
47 9. R. A. Shelby, D. R. Smith and S. Schultz, *Science*, 2001, **292**, 77-79.
48
49
50 10. C. Genet and T. W. Ebbesen, *Nature*, 2007, **445**, 39-46.
51
52
53 11. G. M. Crouch, D. Han and P. W. Bohn, *J. Phys. D*, 2018, **51**, 193001.
54
55
56
57
58

12. H. Liu and P. Lalanne, *Nature*, 2008, **452**, 728-731.
13. J. Hennessy, A. D. Jewell, M. E. Hoenk, D. Hitlin, M. McClish, A. G. Carver, T. J. Jones and S. Nikzad, *SPIE Commercial + Scientific Sensing and Imaging*, SPIE, 2017, 10209.
14. R. Gordon, D. Sinton, K. L. Kavanagh and A. G. Brolo, *Acc. Chem. Res.*, 2008, **41**, 1049-1057.
15. J. Yang, G. Duan and W. Cai, *J. Phys. Chem. C*, 2009, **113**, 3973-3977.
16. S. H. Lee, K. C. Bantz, N. C. Lindquist, S.-H. Oh and C. L. Haynes, *Langmuir*, 2009, **25**, 13685-13693.
17. X. Zhang, C. R. Yonzon and R. P. Van Duyne, *J. Mater. Res.*, 2006, **21**, 1083-1092.
18. G. Wang, X. Chen, S. Liu, C. Wong and S. Chu, *ACS Nano*, 2016, **10**, 1788-1794.
19. S. E. Fosdick, K. N. Knust, K. Scida and R. M. Crooks, *Angew. Chem. Int. Ed.*, 2013, **52**, 10438-10456.
20. J. P. Guerrette, S. M. Oja and B. Zhang, *Analyt. Chem.*, 2012, **84**, 1609-1616.
21. G. Loget, D. Zigah, L. Bouffier, N. Sojic and A. Kuhn, *Acc. Chem. Res.*, 2013, **46**, 2513-2523.
22. C. Ulrich, O. Andersson, L. Nyholm and F. Bjorefors, *Angew. Chem. Int. Ed.*, 2008, **47**, 3034-3036.
23. W. Xu, K. Fu, C. Ma and P. W. Bohn, *Analyst*, 2016, **141**, 6018-6024.

- 1
2
3 24. W. Xu, K. Fu and P. W. Bohn, *ACS Sensors*, 2017, **2**, 1020-1026.
4
5
6 25. C. Park, S. Seo, H. Shin, B. D. Sarwade, J. Na and E. Kim, *Chem. Sci.*, 2015, **6**, 596-602.
7
8
9 26. J.-F. Masson, M.-P. Murray-Méthot and L. S. Live, *Analyst*, 2010, **135**, 1483-1489.
10
11
12
13 27. J. Hu, K. Fu and P. W. Bohn, *Analyt. Chem.*, 2018, **90**, 2326-2332.
14
15
16 28. J. H. Kim and P. J. Moyer, *Opt. Expr.*, 2006, **14**, 6595-6603.
17
18
19 29. J. Zhang, M. Irannejad, M. Yavuz and B. Cui, *Nanoscale Research Letters*, 2015, **10**,
20 238.
21
22
23
24 30. A. Rudenko, C. Mauclair, F. Garrelie, R. Stoian and J. P. Colombier, *Applied Surface*
25 *Science*, 2019, **470**, 228-233.
26
27
28
29 31. M. Irannejad, M. Yavuz and B. Cui, *Photon. Res.*, 2013, **1**, 154-159.
30
31
32
33 32. L. I. B. Silva, M. Freitas, T. A. P. Rocha-Santosa and A. C. Duarte, *Talanta*, 2010, **82**,
34 1403-1411.
35
36
37
38
39
40
41
42
43
44
45
46
47
48
49
50
51
52
53
54
55
56
57
58
59
60

Figures

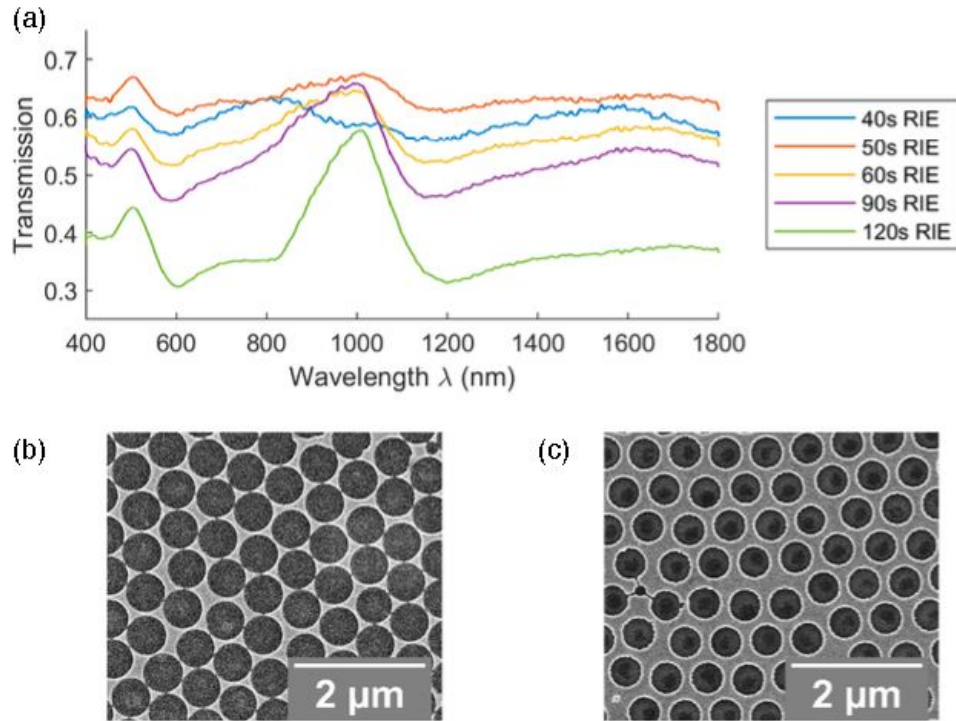


Figure 1. (a) Optical transmission spectra of nanoaperture metamaterials obtained at 600 nm spacing using increasing O_2 plasma etch times, resulting in smaller apertures at constant center-to-center spacing. Plan view scanning-electron microscope (SEM) images of nanoaperture metamaterials obtained with (b) 30 s and (c) 2 min RIE times.

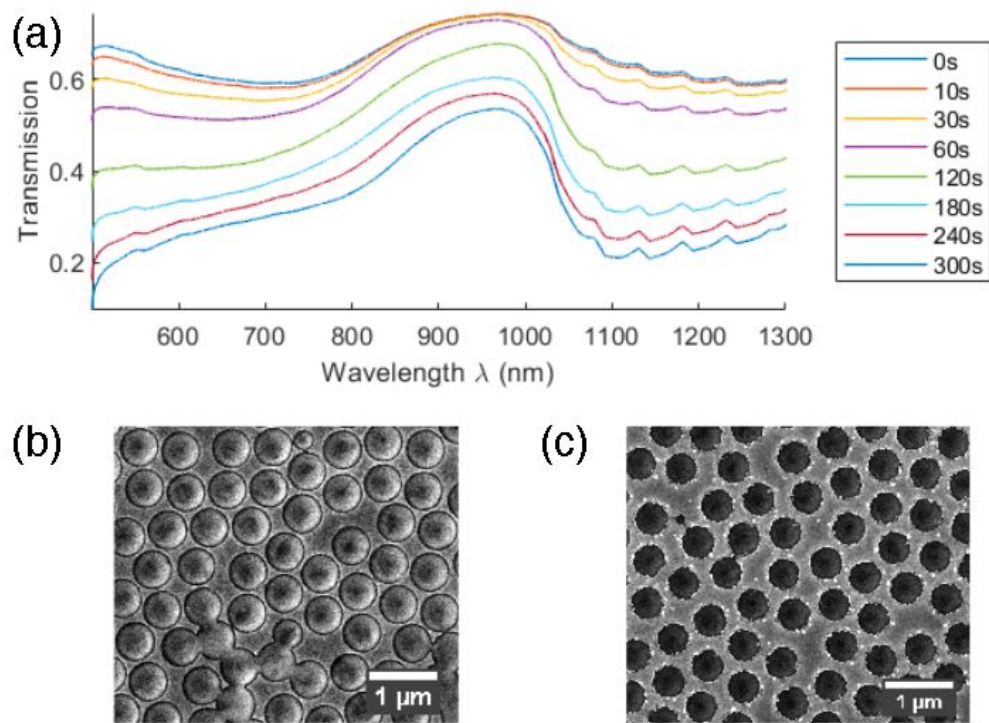


Figure 2. (a) Transmission spectra of a nanoaperture metamaterial (600 nm spacing, 50s O_2 plasma etch) reporter cell showing post-fabrication tuning of nanoaperture metamaterial transmission spectra by galvanostatic application of 20 μA for increasing times. SEM images of the sample before (b) and after (c) showing hole shrinkage and smoothness of deposited Ag layer. EDX images are given in **Figures S4** and **S5** before and after deposition, respectively.

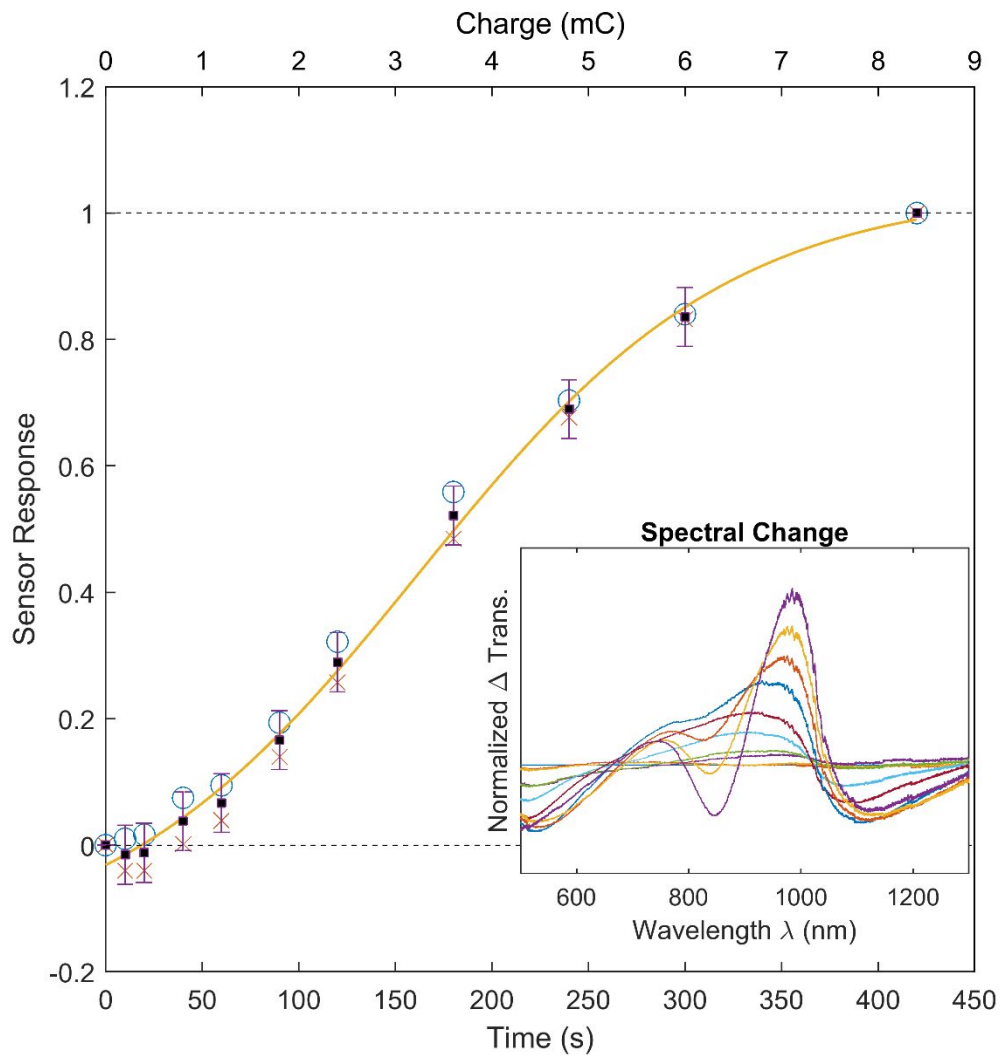


Figure 3. Plot of sensor response vs. time during a galvanostatic deposition ($2 \mu\text{A}$) in a nanoaperture metamaterial reporter cell. Spectral response is calculated from the best-fit linear combination of starting and ending normalized spectra (x, red), while intensity response is based on the overall change in normalized transmittance (open circles, blue.) A sigmoidal response curve fit to the average of the two responses (squares, black) is given by the yellow line, with error bars $\pm 3\sigma$. (Inset) Normalized transmission difference (compared to the $t = 0$, $Q = 0$ spectrum) spectra.

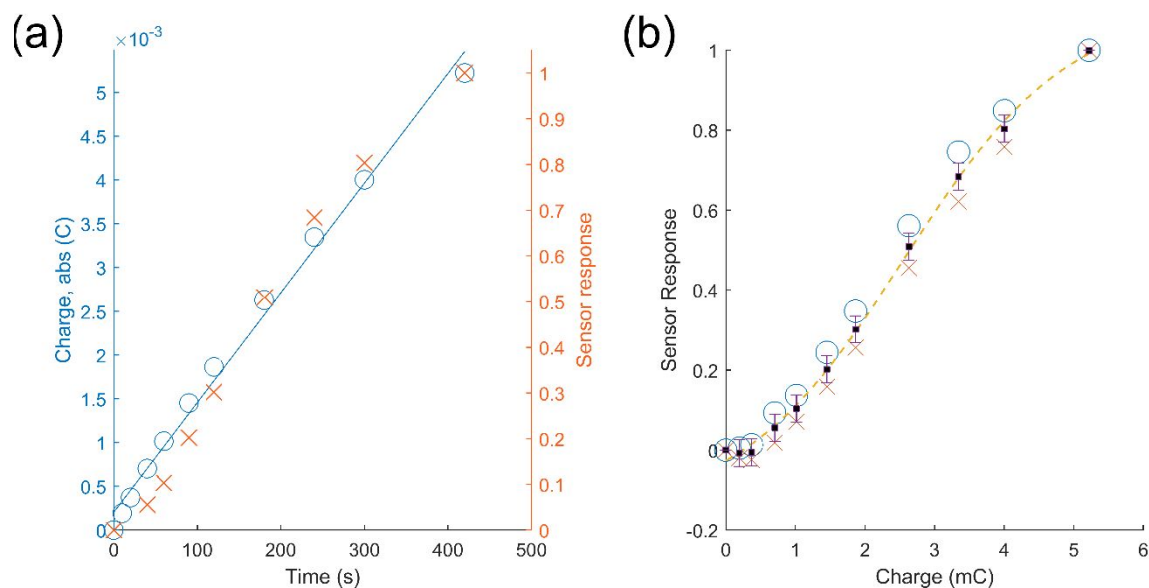


Figure 4. CBE sensor device operation with 1 mM $\text{Fe}(\text{CN})_6^{4-}$ analyte, showing reporter cell response during constant potential application, -2.0 V Pt WE (analyte cell) vs. ITO QRCE (reporter cell), from $t = 0$ s - 420 s. (a) Charge transfer (blue circles, left axis) measured by external potentiostat, with best-fit linear regression (blue line, solid) and corresponding sensor response (red x, right axis). (b) Separate spectral response from best-fit linear combination (x, red) and intensity response corresponding to decrease in transmittance (open circles, blue) are shown as a function of the charge transfer. A sigmoidal response curve fit to the average of the two responses (squares, black) is given by the yellow line, with error bars representing $\pm 3\sigma$.

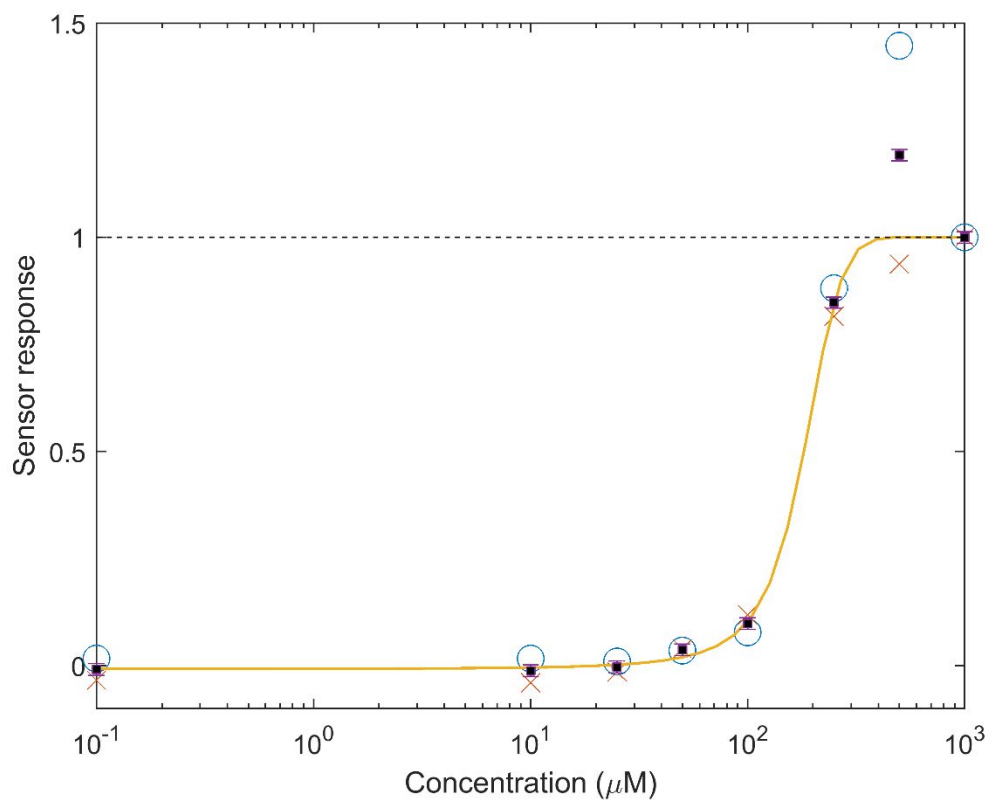


Figure 5. Proof-of-concept experiment showing sensor response as a function of concentration for $\text{Fe}[(\text{CN})_6]^{4-}$. The concentration behavior is obtained from a combined fit to the spectral (x, red) and intensity (open circles, blue) responses after application of -2.0 V vs. analyte cell Pt QRCE for 420 s. A sigmoidal response curve fit to the average of the two responses (squares, black), excluding the $500 \mu\text{M}$ outlier, is given by the yellow line, with error bars $\pm 3\sigma$ estimated from the first three concentrations.

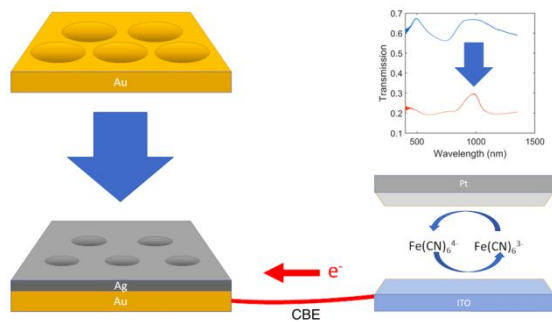
Table 1. Extended Range Sensor Response

| Concentration | Average Sensor Response (a.u.) | Difference ^b |
|--------------------|--------------------------------|-------------------------|
| 1 nM | -0.11 | ±0.11 |
| 100 nM | 0.12 | ±0.07 |
| 1 μM | 0.81 | ±0.07 |
| 10 μM ^a | 1.00 ^a | NA ^a |

^aThis concentration was used to define the saturated sensor response, S_{final} .

^bDifference between average and spectral/intensity responses.

Table of Contents Graphic



Summary Statement

Closed bipolar electrochemistry to couple an analytical reaction to an optical readout by the reconfiguration of an optical metamaterial.